

ORIGINAL RESEARCH

# Inhibition of Aryl Hydrocarbon Receptor Attenuates Hyperglycemia-Induced Hematoma Expansion in an Intracerebral Hemorrhage Mouse Model

Reng Ren , MD\*; Qin Lu , MD\*; Prativa Sherchan, PhD; Yuanjian Fang , MD; Cameron Lenahan , BS; Lihui Tang , MD; Yi Huang , MD; Rui Liu, MD; John H. Zhang , MD, PhD; Jianmin Zhang, MD, PhD; Jiping Tang , MD, PhD

**BACKGROUND:** Hyperglycemia is associated with greater hematoma expansion (HE) and worse clinical prognosis after intracerebral hemorrhage (ICH). However, the clinical benefits of intensive glucose normalization remain controversial, and there are no approved therapies for reducing HE. The aryl hydrocarbon receptor (AHR) has been shown to participate in hyperglycemia-induced blood–brain barrier (BBB) dysfunction and brain injury after stroke. Herein, we investigated the role of AHR in hyperglycemia-induced HE in a male mouse model of ICH.

**METHODS AND RESULTS:** CD1 mice (n=387) were used in this study. Mice were subjected to ICH by collagenase injection. Fifty percent dextrose was injected intraperitoneally 3 hours after ICH. AHR knockout clustered regularly interspaced short palindromic repeat was administered intracerebroventricularly to evaluate the role of AHR after ICH. A selective AHR inhibitor, 6,2',4'-trimethoxyflavone, was administered intraperitoneally 2 hours or 6 hours after ICH for outcome study. To evaluate the effect of AHR on HE, 3-methylcholanthrene, an AHR agonist, was injected intraperitoneally 2 hours after ICH. The results showed hyperglycemic ICH upregulated AHR accompanied by greater HE. AHR inhibition provided neurological benefits by restricting HE and preserving BBB function after hyperglycemic ICH. In vivo knockdown of AHR further limited HE and enhanced the BBB integrity. Hyperglycemia directly activated AHR as a physiological stimulus in vivo. The thrombospondin-1/transforming growth factor- $\beta$ /vascular endothelial growth factor axis partly participated in AHR signaling after ICH, which inhibited the expressions of BBB-related proteins, ZO-1 and Claudin-5.

**CONCLUSIONS:** AHR may serve as a potential therapeutic target to attenuate hyperglycemia-induced hematoma expansion and to preserve the BBB in patients with ICH.

**Key Words:** blood ■ hyperglycemia ■ intracerebral hemorrhage

Intracerebral hemorrhage (ICH) has the highest risk of fatality among all types of stroke with a 30-day mortality rate of 40%, even in 2019.<sup>1</sup> Approximately one third of patients with ICH develop early hematoma expansion (HE), and mortality increases by 5% with each millimeter of HE.<sup>2</sup> Given that, attempts to limit HE have

drawn substantial attention to develop therapeutics for decades.<sup>3</sup> Currently, there are no approved therapies for reducing HE.<sup>4</sup> While several clinical observational studies have shown that hyperglycemia at the time of admission<sup>5</sup> as well as sustained hyperglycemia after ICH<sup>6</sup> were related to the presence and severity of

Correspondence to: Jiping Tang, 11041 Campus St, Riskey Hall, Room 219, Loma Linda, CA 92354. E-mail: jtang@llu.edu and Jianmin Zhang, 88 Jiefang Rd, Hangzhou, 310009, Zhejiang, China. E-mail: zjm135@zju.edu.cn

\*R. Ren and Q. Lu contributed equally.

Supplementary Material for this article is available at <https://www.ahajournals.org/doi/suppl/10.1161/JAHA.121.022701>

For Sources of Funding and Disclosures, see page 11.

© 2021 The Authors. Published on behalf of the American Heart Association, Inc., by Wiley. This is an open access article under the terms of the Creative Commons Attribution-NonCommercial-NoDerivs License, which permits use and distribution in any medium, provided the original work is properly cited, the use is non-commercial and no modifications or adaptations are made.

JAHA is available at: [www.ahajournals.org/journal/jaha](http://www.ahajournals.org/journal/jaha)

## CLINICAL PERSPECTIVE

### What Is New?

- Hyperglycemia increased the magnitude of hematoma expansion during experimental intracerebral hemorrhage, and this effect was mediated by the aryl hydrocarbon receptor.
- A hyperglycemia-sensitive mechanism of aryl hydrocarbon receptor-mediated impairment of blood-brain barrier integrity occurred at least partially via a thrombospondin-1/transforming growth factor- $\beta$ /vascular endothelial growth factor signaling pathway, which contributed to hematoma expansion.

### What Are the Clinical Implications?

- Aryl hydrocarbon receptor may serve as a potential therapeutic target to attenuate hyperglycemia-induced hematoma expansion and to preserve the blood-brain barrier in patients with intracerebral hemorrhage.
- Pharmacological antagonism of the aryl hydrocarbon receptor may ameliorate neurobehavioral function and improve the prognosis of patients with intracerebral hemorrhage.

## Nonstandard Abbreviations and Acronyms

<b>AHR</b>	aryl hydrocarbon receptor
<b>BBB</b>	blood-brain barrier
<b>HE</b>	hematoma expansion
<b>ICH</b>	intracerebral hemorrhage
<b>TGF-<math>\beta</math></b>	transforming growth factor- $\beta$

HE, little is known regarding the effect of hyperglycemia on HE and blood-brain barrier (BBB) dysfunction following ICH. Moreover, despite being nondiabetic, 44.7% of patients with acute ICH later presented with new-onset hyperglycemia,<sup>7</sup> but the clinical benefit of intensive glucose normalization remains controversial. The GISK-UK (glucose insulin in stroke trial, United Kingdom), trial of insulin to control blood sugar after acute stroke using magnetic resonance imaging (MRI) end-points (SELESTIAL), and the stroke hyperglycemia insulin network effort (SHINE) are 3 large randomized controlled trials with the objective of targeting post-stroke hyperglycemia with insulin infusion, which failed to provide benefits to patients with stroke.<sup>8</sup> These studies indicate that interventions to counter the deleterious effect of hyperglycemia-related HE should be explored through other underlying mechanisms.

Aryl hydrocarbon receptor (AHR) is a ligand-activated transcription factor located in the cytoplasm.<sup>9</sup>

AHR is known to be widely expressed in astrocytes, endothelial cells, and neuronal cells in the brain,<sup>10</sup> and it plays important roles in sensing and metabolizing xenobiotic factors such as polyaromatic hydrocarbons and environmental toxins with its highly conserved PER-ARNT-SIM domain.<sup>11</sup> As demonstrated by the phenotype in AHR knockout mice,<sup>12</sup> AHR was postulated to be linked with vascular and cardiac homeostasis, immune system function, and neoplasm development in response to endogenous ligands such as kynurenine and tryptophan metabolite under normal cell physiology. The pathophysiological roles of AHR in the central nervous system have been extensively studied.<sup>10</sup> In experimental stroke models, inhibition of AHR was demonstrated to have neuroprotective effects,<sup>13</sup> but the mechanisms underlying BBB protection remain poorly explored. Furthermore, there are no studies that have investigated the role of AHR in HE after ICH.

A recent study showed that AHR was activated in response to high glucose stimulation, which led to the formation of a complex with 2 other glucose-sensitive transcription factors, Egr-1 and AP-2.<sup>14</sup> The active AHR complex was shuttled into the nucleus and activated the glucose-responsive gene promoter fragment of thrombospondin-1<sup>14</sup> by binding to it. Furthermore, the thrombospondin-1/transforming growth factor- $\beta$  (TGF- $\beta$ )/vascular endothelial growth factor (VEGF) pathway<sup>15</sup> has been implicated in BBB breakdown.<sup>16</sup>

Herein, we explored the role of AHR on hematoma expansion after ICH. We investigated the effects of AHR inhibition on hematoma expansion and explored underlying mechanisms of protection pertaining to BBB protection after hyperglycemic ICH in mice (Figure S1).

## METHODS

### Data Availability

All data are available within the article and additional data can be acquired from the corresponding author.

### Reagents

The AHR antagonist, 6,2',4'-trimethoxyflavone (TMF), AHR agonist, 3-methylcholanthrene (3-MC), dimethyl sulfoxide (DMSO), dextrose, and mannitol were from Sigma-Aldrich, MO. LSKL, Thrombospondin (TSP-1) inhibitor, was from MedChem Express, NJ.

### Animal Models and Experimental Design

A total of 387 adult male CD-1 mice (weight 30–35 g, Charles River, Wilmington, MA) aged 8–10 weeks were used for the study. All mice were housed under a 12-hour light/dark cycle with ad libitum access to food and standard water. All animal experimental procedures were approved by the Institutional Animal Care and Use

Committee at Loma Linda University (#8190039) and were compliant with the Animal Research: Reporting In Vivo Experiments (ARRIVE) guidelines. Mice were randomly assigned to different experimental groups by generating random numbers. Information on experimental groups was blinded to researchers who performed surgeries, neurobehavioral assessments, Western blot, immunofluorescence staining, and data analysis. Six separate experiments were conducted (Figure S2). Animal numbers per group are listed in Table S1.

### **Experiment 1. To Investigate the Effect of Hyperglycemia on HE after ICH**

Forty-two mice were assigned to 3 groups: sham, ICH, and ICH+dextrose. Blood glucose and hematoma volume were measured accordingly. Additionally, 6 mice were used to evaluate the impact of hyperosmotic solution on hematoma expansion in the ICH+mannitol group.

### **Experiment 2. To Evaluate Time Course and Cellular Localization of AHR in the Ipsilateral Hemisphere After ICH**

Sixty mice were assigned to the following 9 groups: sham, ICH(6h), ICH(12h), ICH(24h), ICH(72h), ICH+dextrose(6h), ICH+dextrose(12h), ICH+dextrose(24h) and ICH+dextrose(72h). Western blot was performed to evaluate temporal changes in protein expressions, and double immunofluorescence staining was used to explore cellular localization of AHR after ICH.

### **Experiment 3. To Assess the Effect of Treatment with AHR Antagonist TMF on HE, BBB Damage, and Neurobehavioral Outcomes After Hyperglycemic ICH**

Part 1. One hundred sixteen mice were divided into 7 groups: sham, ICH, ICH+dextrose, ICH+dextrose+DMSO, ICH+dextrose+TMF(low dose, 1.5mg/kg), ICH+dextrose+TMF(middle dose, 5mg/kg), ICH+dextrose+TMF(high dose, 15mg/kg). Hematoma volume, neurobehavioral tests, and brain water content were measured at 24 hours and 72 hours after ICH. Tail bleeding time and clot formation ex vivo were also measured. Additionally, 6 mice were used to evaluate neurobehavioral tests and hematoma expansion in the ICH+TMF group.

Part 2: Sixty-four mice were divided into the following 5 groups: sham, ICH, ICH+dextrose, ICH+dextrose+DMSO, and ICH+dextrose+TMF (5 mg/kg). BBB permeability was evaluated using IgG staining, Evan's blue extravasation tests, and Perls' staining. Rotarod tests were conducted on days 0, 7, 14, and 21 after ICH.

### **Experiment 4. To Determine the Role of AHR on HE and BBB Function After Hyperglycemic ICH**

Sixty-six mice were assigned to the following 4 groups: Sham, ICH+dextrose, ICH+dextrose+AHR clustered regularly interspaced short palindromic repeat (CRISPR) knockout, and ICH+dextrose+knockout CRISPR Control. Western blots, hemoglobin assay, Evan's blue extravasation, double immunofluorescence staining, and neurobehavioral tests were measured.

### **Experiment 5. To Explore Hyperglycemia Interaction with AHR and HE After ICH**

Thirty-six mice were assigned to 3 groups: ICH, ICH+dextrose, and ICH+3-MC. Immunoprecipitation was performed to detect the interaction between AHR with Egr-1.

### **Experiment 6. To Determine Potential Deleterious Molecular Mechanism of AHR-Mediated BBB Disruption and HE Expansion After Hyperglycemic ICH**

Fifty-four mice were assigned to 9 groups: sham, ICH+dextrose, ICH+dextrose+DMSO, ICH+dextrose+TMF, ICH+dextrose+TMF+CRISPR Control, ICH+dextrose+TMF+thrombospondin-1 CRISPR activation, ICH+dextrose+3-MC, ICH+dextrose+3-MC+DMSO, and ICH+dextrose+3-MC+LSKL. Western blots were used to evaluate the protein expression changes.

### **Collagenase-Induced ICH Model and Hyperglycemia Procedure**

The collagenase injection ICH model was performed as described previously.<sup>17</sup> Briefly, the mice were weighed and anesthetized with a ketamine-xylazine cocktail (1.5 mL/kg). Next, the animals were fixed to a stereotactic frame in a prone position and the position of the Hamilton syringe was adjusted to ensure proper injection site relative to bregma (right lateral 2.2 mm, rostral 0.2 mm). A burr hole was drilled at the position. Next, the infusion pump was set at a rate of 0.2  $\mu$ L/min and the needle of the Hamilton syringe was advanced ventrally to a depth of 3.5 mm to infuse 1  $\mu$ L collagenase (0.075 U). The needle was left in situ for 5 minutes after the end of infusion before retracting at a rate of 1 mm/min. Sham group mice were subjected to a similar procedure but received 0.9% sterile saline injection. Three hours after ICH induction, the mice were injected with 6 mL/kg of 50% dextrose intraperitoneally. Baseline and follow-up blood glucose levels up to 8 hours postsurgery were measured using a glucometer (ReliOn) in tail vein blood.

## Neurobehavioral Tests

The modified Garcia neurological score, corner turn test, forelimb placement test, and Rotorod test were used to assess neurobehavioral function.<sup>18</sup>

## Brain Water Content Measurement

Wet–dry weight measurement for brain edema was performed as previously reported.<sup>19</sup> Brain water content (%) was calculated as (wet weight–dry weight)/wet weight\*100%.

## Intracerebroventricular Injection

As previously described,<sup>20</sup> intracerebroventricular injection in the left ventricle was performed using the coordinates left lateral of bregma=1.0 mm and ventral depth=3.2 mm. For each of the CRISPRs, a total of 2  $\mu$ L CRISPR (final concentration 0.5  $\mu$ g/ $\mu$ L) was injected into the left lateral ventricle 48 hours before ICH. The detailed procedure is shown in Data S1.

## Western Blots and Immunoprecipitation Assay

Western blots and immunoprecipitation assay were performed as reported previously.<sup>21</sup> The antibodies used are listed in Table S2. Western blot bands were quantified as relative density of bands using Image J software (NIH, Bethesda, USA).

## Hemoglobin Assay and Image-Based Measurement of Hematoma Volume

A modified spectrophotometric assay was used to measure hemoglobin content, and a step-by-step procedure for hematoma volume measurement was followed as per a previously published protocol.<sup>22</sup>

## Tail Bleeding Monitoring and Ex Vivo Thrombus Formation

Hemostasis was assessed by measuring bleeding time using the tail transection test as described previously.<sup>23</sup> Details of the procedure are shown in Data S1.

## Evan's Blue Dye Extravasation

Evan's blue extravasation was used to evaluate BBB disruption as reported before.<sup>24</sup> The optical density was measured at 610 nm.

## Immunohistochemistry

Immunofluorescence staining was performed on frozen brain sections as reported previously.<sup>21</sup> The antibodies used are listed in Table S2. Immunohistochemistry staining for IgG was performed using VECTASTAIN

ABC Kit (Peroxidase-HRP, PK-4002, VECTOR Laboratories).

Perls' staining was conducted using IRON STAIN Kit (HT 20, Sigma-Aldrich) following the procedure suggested by the manufacturer. All the morphological results were photographed using a Zeiss microscope equipped with a digital color camera.

## Statistical Analysis

All data analysis was performed using GraphPad Prism 8.2.1 (GraphPad Software, CA) and data were expressed as mean $\pm$ SD. Multiple comparisons were statistically analyzed with Kruskal–Wallis test followed by post hoc Dunn's method or 2-way ANOVA followed by the post hoc Tukey method. Statistical significance was defined as  $P<0.05$ .

## RESULTS

### Hyperglycemia Exacerbated Hematoma Expansion After ICH

The hyperglycemic ICH group had a significantly larger hematoma compared with the ICH-only group ( $P<0.05$ , Figure 1A through 1C). TMF did not have any effect on plasma glucose levels. Hyperosmotic 20% mannitol did not significantly affect HE (Figure S3B and S3C).

### AHR Was Upregulated and Expressed in Astrocytes and Endothelial Cells After Hyperglycemic ICH

Temporal AHR expression after hyperglycemic ICH was upregulated at  $\approx$ 6 hours and peaked at 24 hours ( $P<0.05$ , Figure 1D and 1E). AHR mainly localized in perivascular astrocytes as well as in endothelial cells after hyperglycemic ICH (Figure 1F).

### TMF Attenuated HE, and Improved Short- and Long-Term Outcomes in Hyperglycemic ICH Mice

#### *TMF Limited HE and Improved Neurobehavioral Function*

TMF was administered in a dose-gradient manner 2 hours after ICH. TMF 5 mg/kg significantly attenuated HE, and exhibited better neurobehavioral function and less brain water content at 24 hours after hyperglycemic ICH. Given these findings, only the 5 mg/kg dose of TMF was used to evaluate outcomes at 72 hours and for rest of the experiments. Seventy-two hours after hyperglycemic ICH, TMF 5 mg/kg improved neurobehavioral function, attenuated HE, and alleviated BWC in ipsilateral basal ganglia and cortex ( $P<0.05$ , Figure 2A and 2B).

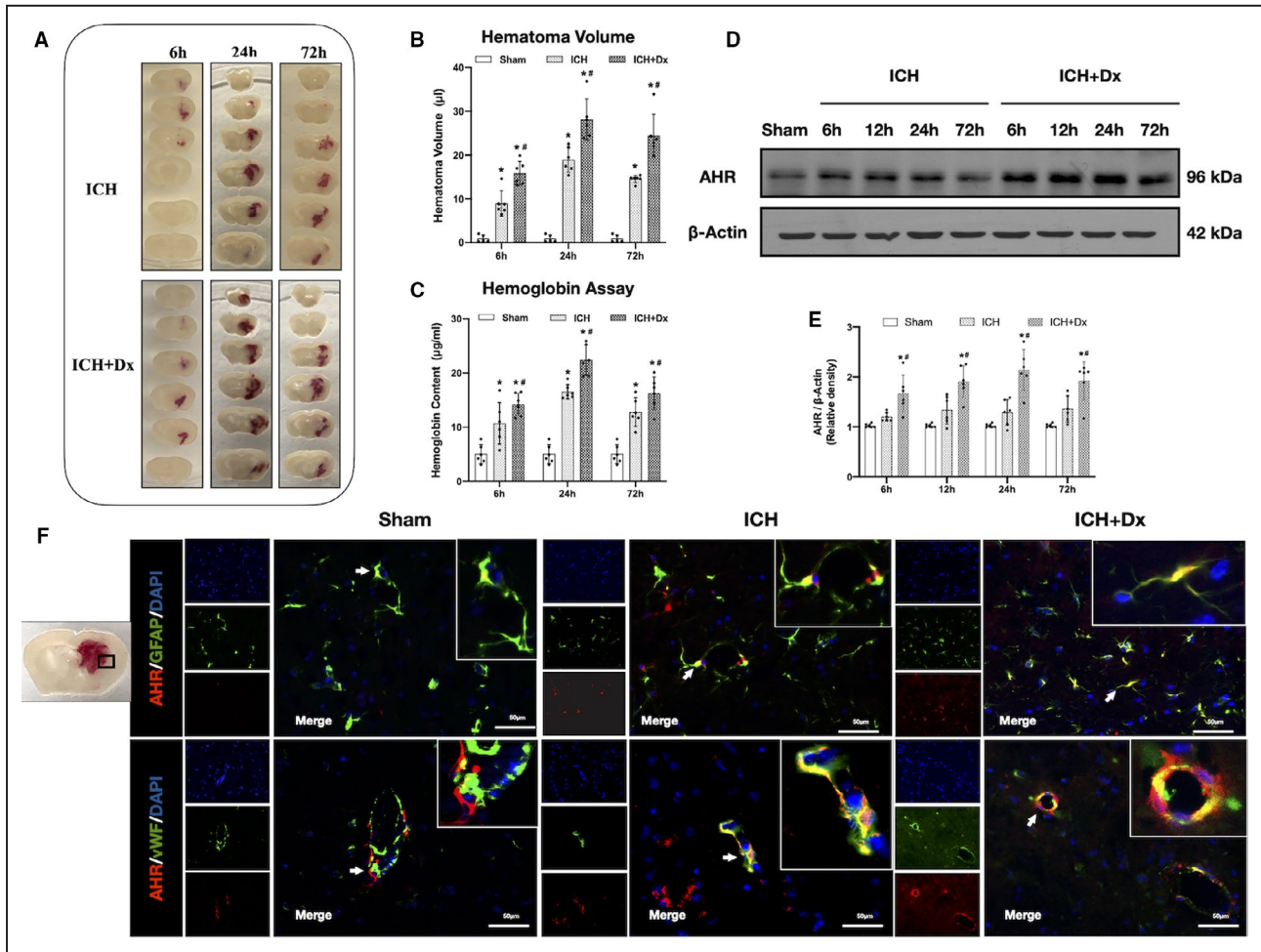


**Figure 1.** Formation of hematoma expansion accompanied with temporal expression of AHR and cellular localization in hyperglycemic ICH mice.

**A**, Photographs of mice brain coronal sections of 1-mm thickness in ICH and ICH+Dx groups at 6, 24, and 72 hours after ICH. **B** and **C**, Statistical analysis of hematoma volume and hemoglobin assay. **D**, Representative Western blot bands of AHR at 6, 12, 24, and 72 hours in ICH group and ICH+Dx group. **E**, Quantitative analysis of AHR. **F**, Double immunofluorescence staining for AHR (red) with astrocyte (GFAP, green), endothelial cell (vWF, green) around the hematoma at 24 hours in different groups.  $n=2$  per group. Scale bar, 50  $\mu\text{m}$ . AHR indicates aryl hydrocarbon receptor; DAPI, 4',6-diamidino-2-phenylindole; Dx, dextrose; GFAP, glial fibrillary acidic protein; ICH, intracerebral hemorrhage; and vWF, von Willebrand factor. The error bars represent mean $\pm$ SD. \* $P<0.05$  vs Sham. # $P<0.05$  vs ICH. Two-way ANOVA, Tukey's test.  $n=6$  for each group.

Delayed TMF administration (5 mg/kg administered at 6 hours after ICH) also significantly limited HE and improved neurological function at 24 hours after hyperglycemic ICH ( $P<0.05$ , Figure 2C). Additionally, TMF had no effect on hemostasis in vivo and ex vivo (Figure S4C).

### TMF Alleviated BBB Impairment and Improved Long-Term Neurobehavioral Outcome

Hyperglycemic ICH mice receiving TMF (5 mg/kg) demonstrated a lesser extent of BBB leakage and ferric iron deposition around the perihematomal region in basal ganglion ( $P<0.05$ , Figure 3A through 3C, and 3E). Likewise, TMF 5 mg/kg improved long-term

sensorimotor and balance function at 1 to 3 weeks after ICH (Figure 3D).

### Effect of AHR Knockout in Hyperglycemic ICH Mice

To verify in vivo AHR CRISPR knockout efficacy, mice were subjected to AHR CRISPR knockout, which showed significantly decreased expression of AHR as well as downstream proteins thrombospondin-1, TGF- $\beta$ , and VEGF while ZO-1 was upregulated compared with control CRISPR ( $P<0.05$ , Figure 4A) In vivo AHR CRISPR knockout ameliorated HE and preserved BBB disruption, thus improving neurobehavioral function

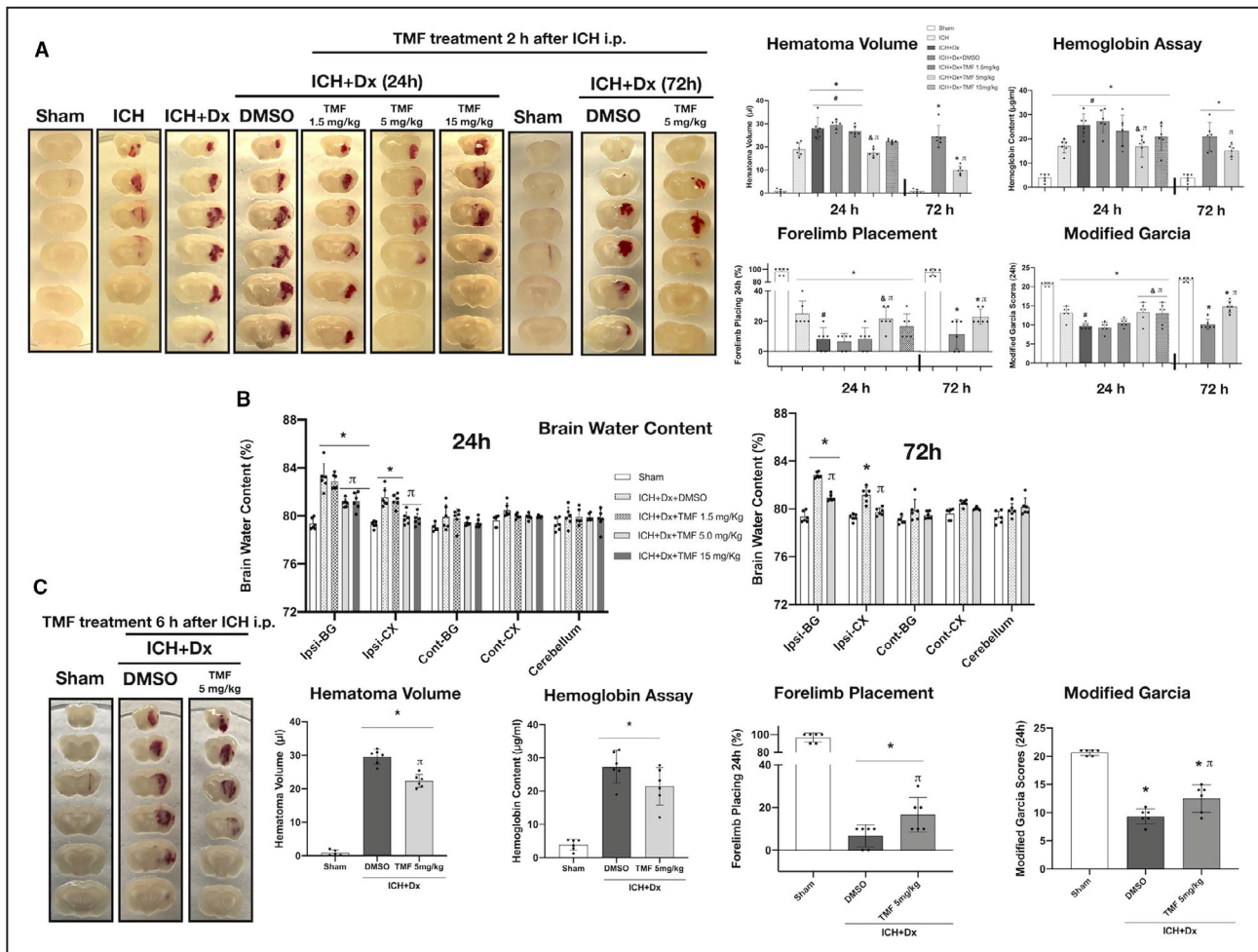


**Figure 2.** Inhibition of AHR by TMF attenuated hematoma expansion, alleviated brain edema, and improved neurobehavioral outcomes at 24 hours and 72 hours after hyperglycemic ICH.

**A**, Photographs of mice brain coronal sections of 1-mm thickness in different groups at 24 hours and 72 hours after hyperglycemic ICH. Statistical analysis of hematoma volume and hemoglobin assay. Neurobehavioral testing using modified Garcia test and forelimb placing test in different groups. Kruskal–Wallis test followed by post hoc Dunn’s test. **B**, Statistical analysis of brain water content at 24 hours and 72 hours after hyperglycemic ICH in different brain regions. Two-way ANOVA, Tukey’s test. **A** and **B**, TMF was given intraperitoneally 2 hours after collagenase injection. **C**, Photographs of mice brain coronal sections of 1-mm thickness in different groups at 24 hours after hyperglycemic ICH. Statistical analysis of hematoma volume and hemoglobin assay. Neurobehavioral testing using modified Garcia test and forelimb placing test in different groups. Kruskal–Wallis test followed by post hoc Dunn’s test. TMF was given 5 mg/kg ip 6 hours after collagenase injection and outcomes were evaluated at 24 hours after ICH. AHR indicates aryl hydrocarbon receptor; BG, Basal Ganglia; Cx, Cortex; DMSO, dimethyl sulfoxide; Dx, dextrose; ICH, intracerebral hemorrhage; and TMF, trimethoxyflavone. The error bars represent mean±SD. \* $P<0.05$  vs sham. # $P<0.05$  vs ICH. & $P<0.05$  vs ICH+Dx.  $\pi$   $P<0.05$  vs ICH+Dx+DMSO.  $n=6$  for each group.

after hyperglycemic ICH ( $P<0.05$ , Figure 4B through 4D).

### Hyperglycemia-Activated AHR and Aggravated HE After ICH

The interaction of AHR with Egr-1 was significantly increased in hyperglycemic ICH mice compared with sham and ICH mice ( $P<0.05$ , Figure 5A and 5B). ICH mice subjected to either dextrose or 3-MC induced a similar severity of HE and BBB leakage (Figure 5C through 5E).

### AHR Modulated BBB Dysfunction Through Activation of Thrombospondin-1/TGF- $\beta$ /VEGF Signaling Pathway

The temporal expression patterns of thrombospondin-1, TGF- $\beta$ , and VEGF, as AHR-related signaling downstream pathway proteins, were consistent with the time course expression of AHR (Figure S5).

At 24 hours after hyperglycemic ICH, TMF significantly decreased the expression of AHR, thrombospondin-1, TGF- $\beta$ , and VEGF, whereas ZO-1 and Claudin-5 protein expression increased. Thrombospondin-1

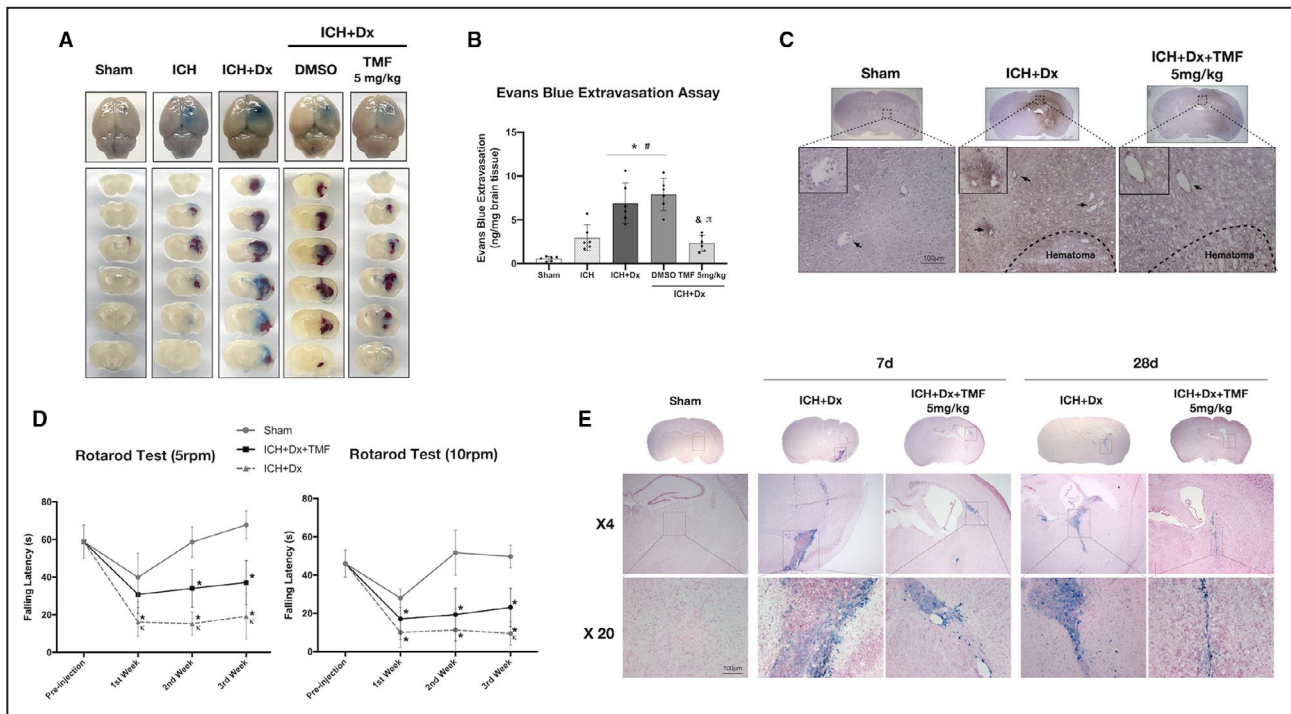


**Figure 3. Inhibition of AHR by TMF alleviated blood–brain barrier damage and iron deposition at short and long term after hyperglycemic ICH.**

**A**, Photographs of mice brain coronal sections of 1-mm thickness in different groups with Evan's Blue injection ip. **B**, Quantitative measurement of Evan's Blue extravasation. Kruskal–Wallis test followed by post hoc Dunn's test.  $n=6$  for each group. **C**, Photographs of mice brain coronal sections; micrographs indicate representative immunostaining with mouse IgG from each group. **D**, Rotarod test (5 rpm and 10 rpm) evaluated on the first, second, and third weeks after ICH. Two-way ANOVA, Tukey's test.  $n=4$  for each group. **E**, Representative photos of Perls' staining in the ipsilateral basal ganglia. Blue spots represented deposited iron. Scale bar=100  $\mu$ m. AHR indicates aryl hydrocarbon receptor; DMSO, dimethyl sulfoxide; Dx, dextrose; ICH, intracerebral hemorrhage; TMF, trimethoxyflavone; and RPM, revolutions per minute. The error bars represent mean $\pm$ SD. \* $P<0.05$  vs Sham. # $P<0.05$  vs ICH.  $\delta P<0.05$  vs ICH+Dx.  $\pi P<0.05$  vs ICH+Dx+DMSO.  $\kappa P<0.05$  vs ICH+Dx+TMF. Black arrows in panel C represent for the microvessels that zoom in onto the upper left corner.

CRISPR activation significantly reversed the aforementioned protein expression except for AHR, which showed no such changes ( $P<0.05$ , Figure 6A and 6B). Likewise, 3-MC augmented the expression of thrombospondin-1, TGF- $\beta$ , VEGF, and diminished ZO-1, Claudin-5, and these changes were reversed with LSKL ( $P<0.05$ , Figure 6C and 6D).

## DISCUSSION

Since the first clinical account of HE was observed and documented in 1937,<sup>25</sup> clinicians have long sought aggressive intervention for HE. Hyperglycemia is associated with greater HE and poorer clinical outcomes after ICH.<sup>26</sup> However, it is more important to demonstrate causation from mechanism to effect rather than correlation. AHR emerged initially as a novel class of protein, an orphan receptor that also functions as a transcription factor with important roles in maintaining physiological functions for the immune system, neurological system, and barrier organs.<sup>27</sup> The objective of

this study was to explore whether AHR played a role in hyperglycemia-induced HE, and whether AHR inhibition ameliorates HE after experimental hyperglycemic ICH in mice. Here, we showed that hyperglycemia exacerbated early HE after ICH. Hyperglycemic ICH induced AHR intracellular overexpression primarily in astrocytes and endothelial cells, which participated in HE concomitantly with upregulation of VEGF-mediated BBB disruption. We also reported that high glucose may account for the direct activation of AHR in this setting. To the best of our knowledge, the present study was the first to demonstrate a pathophysiological role of AHR in ICH as well as the first ever to report glucose as a physiological stimulus for AHR in vivo, revealing a potential therapeutic target from the bench to bedside.

Approximately 50% of patients with acute onset of stroke may develop stress-induced hyperglycemia even in the absence of preexisting diabetes,<sup>28</sup> and emerging evidence demonstrates that during admission to the hospital, stress-induced hyperglycemia was associated with early HE and mortality.<sup>29</sup> To mimic stress-induced hyperglycemia and to improve

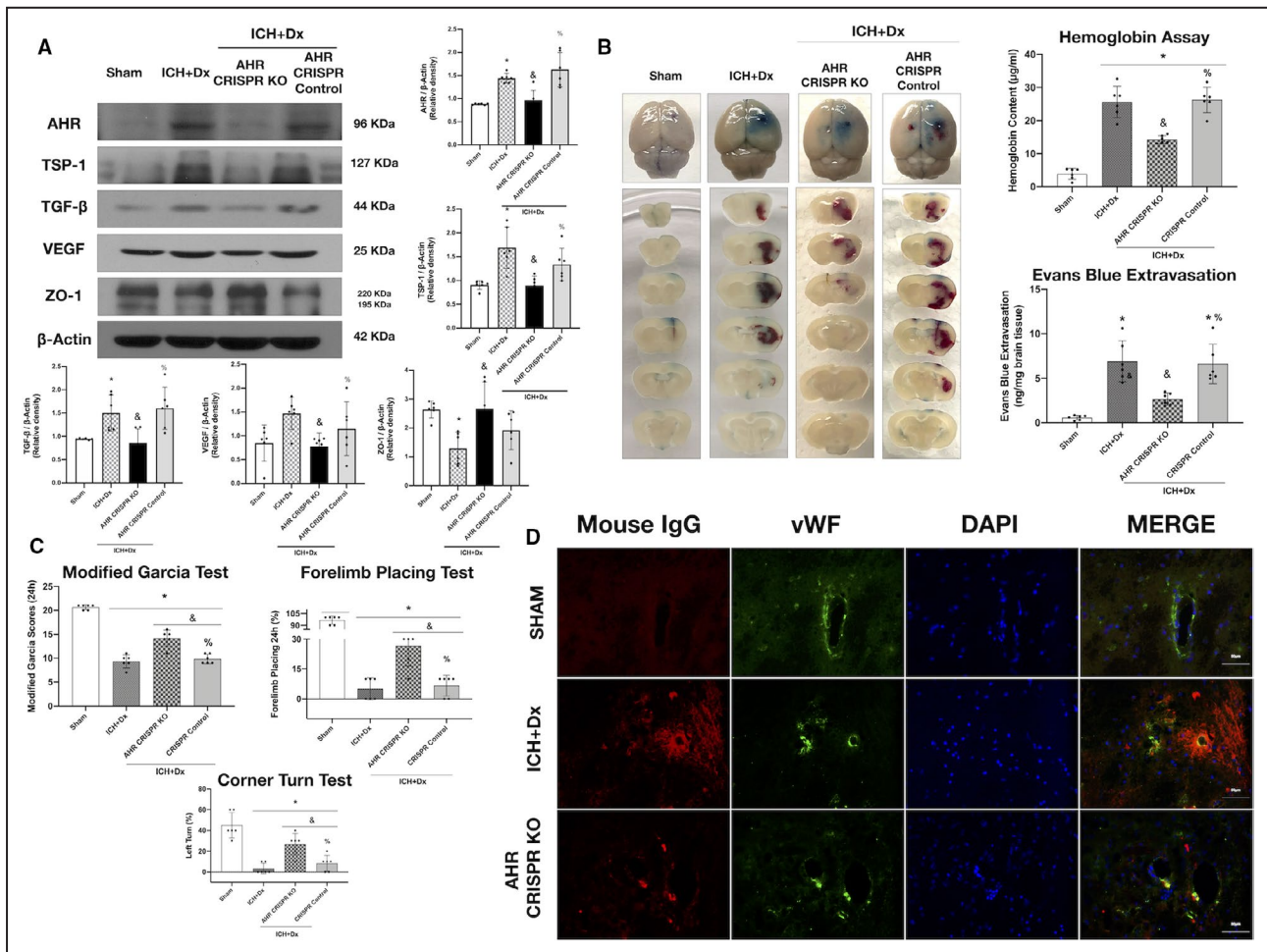


**Figure 4.** In vivo AHR CRISPR knockdown ameliorated hematoma expansion and preserved blood–brain barrier, and thus improved neurobehavioral function after hyperglycemic ICH.

**A**, Representative Western blot bands of AHR and signaling downstream proteins in different groups. Quantitative analysis of AHR, TSP-1, TGF-β, VEGF, ZO-1. **B**, Representative photographs of mice brain coronal sections of 1-mm thickness in different groups with Evan's Blue injection ip (left sided). Quantitative measurement of hemoglobin content and Evan's Blue extravasation (right sided). **C**, Neurobehavioral testing using modified Garcia test, forelimb placing test, and corner turn test in different groups 24 hours after ICH. **D**, Double immunofluorescence staining for mouse IgG (red) with endothelial cells (vWF, green) around the hematoma at 24 hours in different groups after ICH.  $n=2$  per group. Scale bar=50 μm. \* $P<0.05$  vs Sham. &  $P<0.05$  vs ICH+Dx. %  $P<0.05$  vs ICH+Dx+AHR CRISPR KO. The error bars represent mean±SD. Kruskal–Wallis test followed by post hoc Dunn's test.  $n=6$  for each group. AHR indicates aryl hydrocarbon receptor; CRISPR, clustered regularly interspaced short palindromic repeat; DAPI, 4',6-diamidino-2-phenylindole; Dx, dextrose; ICH, intracerebral hemorrhage; KO, knockout; TGF-β, transforming growth factor-β; TSP-1, thrombospondin-1; VEGF, vascular endothelial growth factor; vWF, von Willebrand factor; and ZO-1, zonula occludens-1.

the clinical relevance of this study, we gave a single dose of dextrose injection to CD-1 mice 3 hours after ICH onset, which was in accordance with the average time interval from symptom onset to hospital admission or randomization.<sup>28</sup> Other research teams have also explored the effect of hyperglycemia on HE.<sup>30,31</sup> One study compared the hemorrhagic response between streptozotocin-induced diabetic and nondiabetic rats using an autologous blood injection model by quantifying hematoma enlargement using the subarachnoid space expansion as an indicator.<sup>30</sup> Another study injected collagenase to induce ICH and

monitored temporal hematoma formation by magnetic resonance imaging in streptozotocin-treated rats.<sup>31</sup> Regardless of the differences in subject species and high glucose patterns in these studies, our results were consistent with previous studies, which revealed that a greater macroscopic hematoma and increased bleeding volume were observed in the right basal ganglion as early as 6 hours after hyperglycemic ICH. The hematoma volume peaked at 24 hours and plateaued until 72 hours, whereas plasma glucose returned to baseline long before by 8 hours after ICH. Therefore, we highlighted hyperglycemia as a

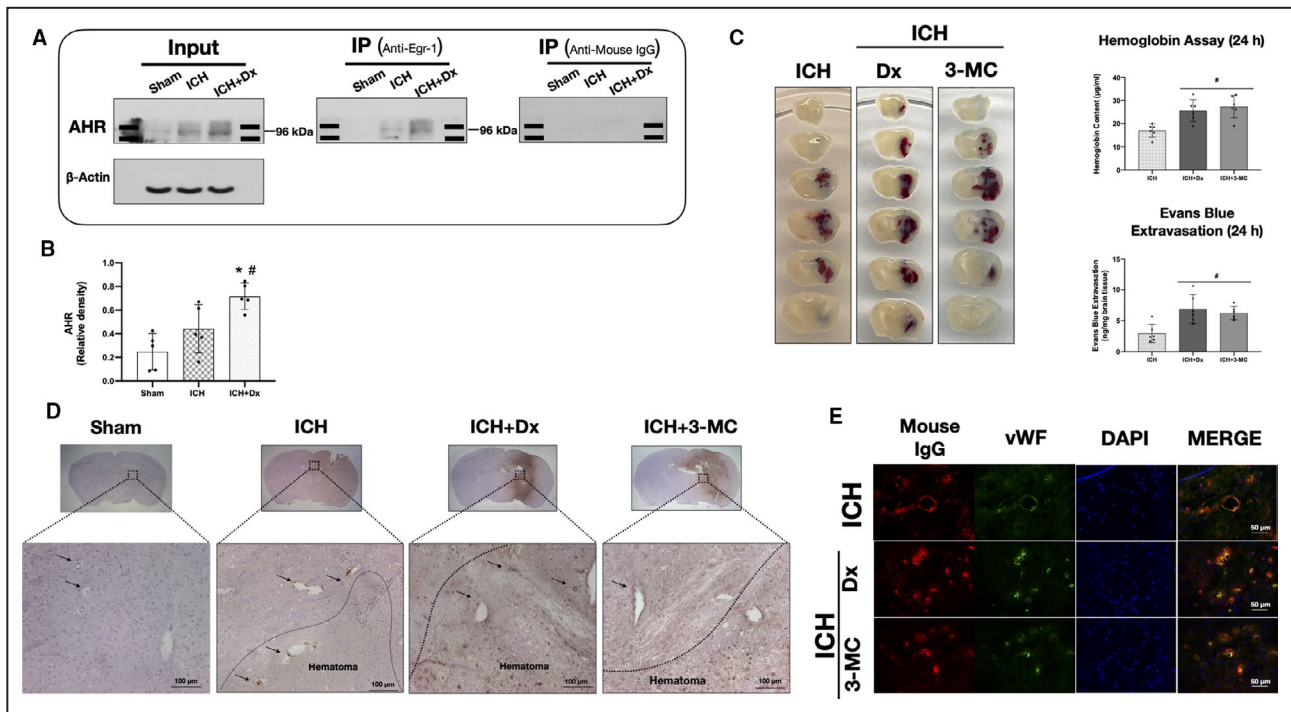


**Figure 5. Hyperglycemia activated AHR and aggravated hematoma expansion after ICH.**

**A**, Immunoprecipitation and **(B)** quantitative analysis of AHR (binding with Egr-1) after Co-IP with Egr-1 antibody at 24 hours in sham, ICH, and ICH+Dx groups. \* $P < 0.05$  vs Sham. # $P < 0.05$  vs ICH. The error bars represent mean  $\pm$  SD. Kruskal–Wallis test followed by post hoc Dunn’s test.  $n = 5$  for each group. **C**, Representative photographs of mice brain coronal sections of 1-mm thickness in different groups with Evan’s Blue injection ip. Quantitative measurement of hemoglobin content and Evan’s Blue extravasation. # $P < 0.05$  vs ICH. The error bars represent mean  $\pm$  SD. Kruskal–Wallis test followed by post hoc Dunn’s test.  $n = 6$  for each group. **D**, Photographs of mice brain coronal sections, micrographs indicate representative immunostaining with mouse IgG from each group. Scale bar = 100  $\mu$ m. **E**, Double immunofluorescence staining for mouse IgG (red) with endothelial cell (vWF, green) around the hematoma at 24 hours in different groups after ICH.  $n = 2$  per group. Scale bar = 50  $\mu$ m. **C** through **E**, 3-MC was injected ip 2 hours after ICH as an AHR agonist to compare the severity of HE and BBB leakage between ICH+Dx and ICH+3-MC groups. AHR indicates aryl hydrocarbon receptor; BBB, blood–brain barrier; Co-IP, co-immunoprecipitation; DAPI, 4’,6-diamidino-2-phenylindole; DMSO, dimethyl sulfoxide; Dx, dextrose; Egr-1, transcription factor early growth response 1; HE, hematoma expansion; ip, intraperitoneal; ICH, intracerebral hemorrhage; 3-MC, 3-methylcholanthrene; and vWF, von Willebrand factor.

triggering factor for HE acting independently of other variables.

Our understanding regarding the scope of AHR-modulated biological and pathophysiological processes has continued to expand, since they were first discovered 2 decades ago<sup>32</sup>. Several studies reported that the expression of AHR was increased during the early<sup>13</sup> and subacute phases of both ischemic and traumatic brain injuries.<sup>33</sup> AHR was detected in the human cerebral microvascular endothelial cell line<sup>34</sup> and astrocytes isolated from the murine BBB. To the best of our knowledge, the present study was the first to show that the AHR signaling pathway was induced in astrocytes and endothelial cells after a deleterious insult such as hemorrhagic stroke.

The early profiles of AHR activation and transcriptional activity strongly suggest a detrimental role of the receptor in the hemorrhagic pathophysiological process. Administration of the specific AHR antagonist TMF limited hematoma enlargement and elicited

better neuroprotective outcomes in a dose-dependent manner in hyperglycemic ICH mice. Conversely, 3-MC, a prototypical AHR agonist, aggravated HE and BBB permeability in ICH mice. Taken together, these findings indicated that AHR played a role in HE after hyperglycemic ICH. The specific AHR antagonist such as TMF may be useful for inhibiting detrimental actions of the receptor after hyperglycemic ICH. However, regulatory roles of AHR in brain pathogenesis are sometimes controversial, which in part may be dependent on the different pharmacological properties of AHR ligands. The partial agonist of AHR, 3,3’-diindolylmethane, may exert an anti-neuroinflammatory effect via activating AHR, and the therapeutic effects of laquinimod, with AHR-activating property, on brain pathology may also be mediated mainly by AHR, although the contribution of AHR-independent actions was not excluded.<sup>35</sup> In line with these previous studies, we found an uptrend of AHR expression between 12 and 72 hours after ICH in mice without dextrose insult, though there was no

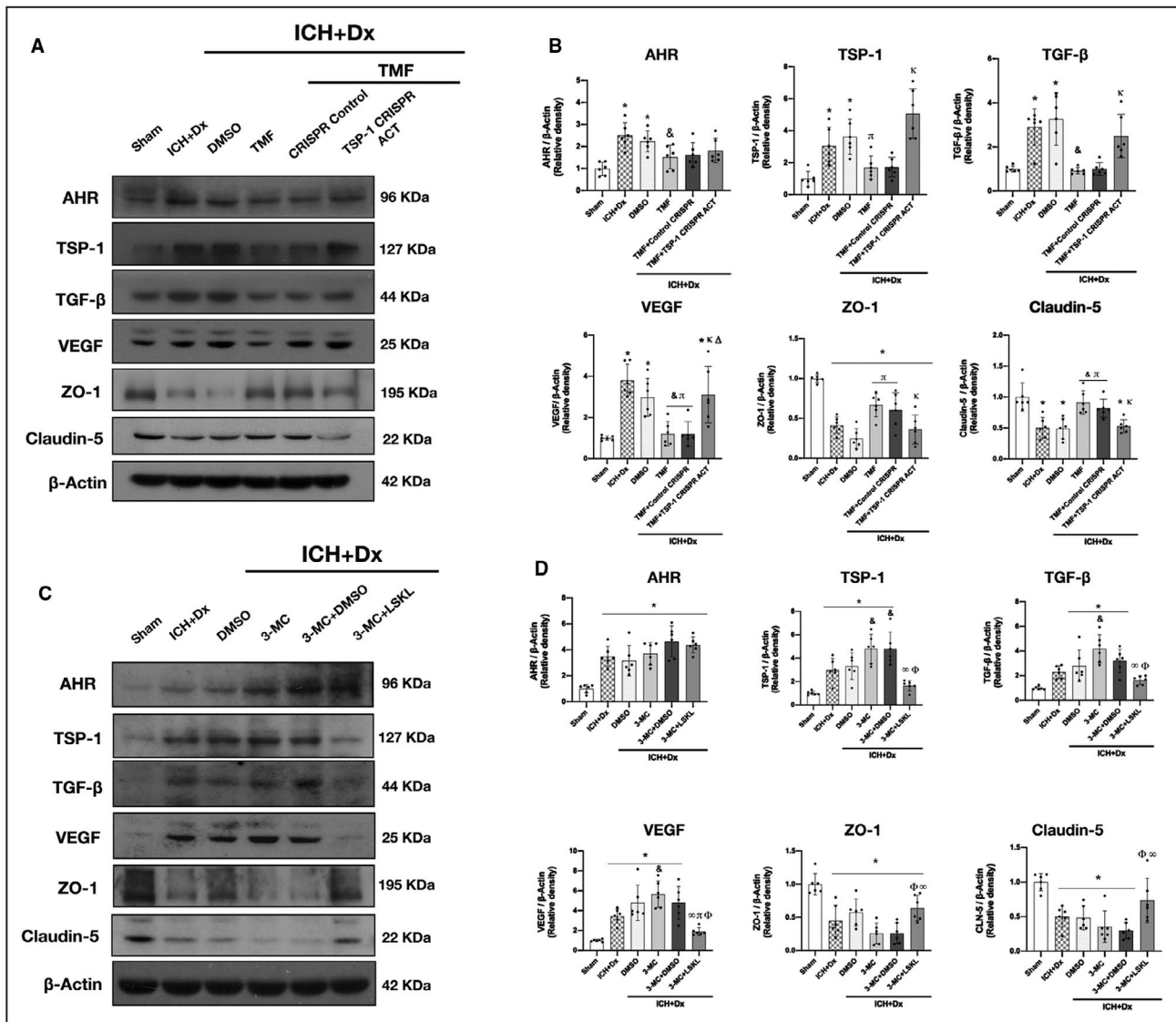


**Figure 6.** In vivo TSP-1 activation CRISPR abolished the effects of TMF and LSKL reversed the activation effects of 3-MC at 24 hours after hyperglycemic ICH.

**A and C.** Representative Western blot bands and quantitative analysis (**B and D**) of AHR and AHR-related downstream signaling pathway proteins (TSP-1, TGF- $\beta$ , and VEGF) and tight junction proteins (ZO-1, CLN-5) at 24 hours in different groups. The error bars represent mean $\pm$ SD. Kruskal–Wallis test followed by post hoc Dunn’s test. \* $P$ <0.05 vs Sham. # $P$ <0.05 vs ICH. & $P$ <0.05 vs ICH+Dx.  $\pi$   $P$ <0.05 vs ICH+Dx+DMSO.  $\kappa$   $P$ <0.05 vs ICH+Dx+TMF.  $\Delta$   $P$ <0.05 vs ICH+Dx+TMF+Control CRISPR.  $\infty$   $P$ <0.05 vs ICH+Dx+3-MC.  $\Phi$   $P$ <0.05 vs ICH+Dx+3-MC+DMSO.  $n=6$  for each group. AHR indicates aryl hydrocarbon receptor; CLN-5, claudin-5; CRISPR, clustered regularly interspaced short palindromic repeat; DMSO, dimethyl sulfoxide; Dx, dextrose; ICH, intracerebral hemorrhage; KO, knockout; LSKL, 3-methylcholanthrene; TGF- $\beta$ , transforming growth factor- $\beta$ ; TMF, trimethoxyflavone; TSP-1, thrombospondin-1; VEGF, vascular endothelial growth factor; and ZO-1, zonula occludens-1.

significant difference between the 2 interventions (ICH versus ICH+TMF) in terms of hematoma volume and short-term outcomes at 24 hours after ICH (Figure S4A and S4B). Further research is warranted for other potential novel endogenous ligands of AHR in response to ICH.

As a crucial pathophysiological feature following ICH, BBB disruption has been considered to be closely involved in HE. However, it remains under debate as to

whether the relationship between BBB and HE after ICH is causative or reciprocal. This study demonstrated that hyperglycemic ICH mice exhibited degradation of ZO-1 and Claudin-5, increased extravasation leakage of Evan’s blue and IgG, and overexpression of VEGF, which indicated more severe BBB damage. Experimental animals as well as human studies have led to the hypothesis that BBB dysfunction may trigger HE after ICH.<sup>36</sup> A systematic review discussing BBB

dysfunction in the pathogenesis of ICH because of cerebral small vessel disease found that there was a temporal relationship between BBB dysfunction and cerebral hemorrhage.<sup>36</sup> BBB disruption markers such as tight junction protein degradation, leakage of contrast agent, plasma protein extravasation, and serum VEGF level indicated vascular injury<sup>36</sup> and predicted subsequent HE.<sup>37</sup> We found that AHR inhibition using TMF increased the expression of tight junction proteins and ameliorated the compromised BBB morphology and function. Taken together, AHR potentiated HE after hyperglycemic ICH through BBB dysfunction, while inhibition of AHR may act as a potential treatment target for HE after hyperglycemic ICH.

We further explored downstream signaling pathway and molecular mechanisms of hyperglycemia-mediated AHR upregulation in ICH. Though few studies have been performed in the hemorrhagic stroke model, several research studies in the ischemic stroke model indicated that pro-inflammatory and anti-neurogenic effects of AHR involved proinflammatory cytokines interleukin-1 $\beta$ , interleukin-6, interferon- $\gamma$ , CXCL1, as well as S100 $\beta$ , NGN2, NGN1 gene and protein expression.<sup>38</sup> AHR also regulated cAMP response element-binding protein survival/death signaling after ischemia, suggesting an anti-apoptosis effect of AHR pharmacological modulation.<sup>13</sup> Additionally, several studies in vivo and in vitro have demonstrated that thrombospondin-1 can activate TGF- $\beta$  endogenously by binding to the latency-associated peptide of TGF- $\beta$ <sup>39</sup> and further induces the phosphorylation of Smad2/3 to its active form, thus promoting the expression of VEGF.<sup>15</sup> Therefore, the thrombospondin-1/TGF- $\beta$ /VEGF axis was suggested to participate in BBB disruption.<sup>15,16</sup> Furthermore, in vitro studies showed that in endothelial cells, AHR was activated and bound to the thrombospondin-1 gene promoter in complex with 2 other nuclear transcription factors, namely, Egr-1<sup>40</sup> and activator protein-2<sup>14</sup> in response to high glucose.<sup>14</sup> We performed an in vivo co-immunoprecipitation experiment that demonstrated direct interaction between AHR and Egr-1. To the best of our knowledge, we are the first to demonstrate in vivo a cascade of events initiated from the activation and overexpression of AHR by hyperglycemia and followed by subsequent upregulation of the thrombospondin-1/TGF- $\beta$ /VEGF axis that participated in BBB dysfunction leading to HE after ICH, thus providing a novel mechanistic insight and therapeutic target for ICH.

## Limitations

There were several limitations to this study. First, the experimental ICH model, which used collagenase injection to induce ICH, does not emulate the cause of

spontaneous ICH in clinical scenarios such as hypertensive vasculopathy and cerebral amyloid angiopathy. Given the challenges inherent in animal models, more studies are necessary to explore the clinical impact regarding the role of AHR in hyperglycemic ICH. Also, we only used young male mice in this study. The rationale for choosing young and male mice was to rule out confounding factors, in this case, sex and age. Given the possibility that there might be different therapeutic and side effects in old or female mice, further studies are warranted to determine sex- and age-dependent effects. Second, we used CRISPR to edit the in vivo genome. Although control CRISPR was also used to exclude potential off-target effects, there may still be some unpredictable off-target effects on neurobehavioral function and protein expression. For further validation of the AHR function, transgenic animals should be considered. Lastly, although this study found that the mechanism of action for AHR was derived from downstream BBB dysfunction, AHR has been shown to exhibit anti-apoptotic effect after ischemic stroke.<sup>13</sup> Therefore, further studies are necessary to elucidate other roles and mechanisms of AHR in ICH.

## CONCLUSIONS

The present study showed that hyperglycemia increased the magnitude of HE during experimental ICH, and this effect was mediated by AHR. A hyperglycemia-sensitive mechanism for AHR-mediated impairment of BBB integrity could contribute to hematoma expansion after ICH. Overall, this study linked hyperglycemia with AHR signaling in ICH and identified AHR as a potential therapeutic target in this setting.

## ARTICLE INFORMATION

Received June 4, 2021; accepted August 27, 2021.

### Affiliations

Department of Neurosurgery (R.R., Y.F., Y.H., J.Z.); and Department of Neurointensive Care Unit (R.R.), The Second Affiliated Hospital, Hangzhou, Zhejiang, China; Department of Physiology and Pharmacology (R.R., Q.L., P.S., Y.F., C.L., L.T., Y.H., R.L., J.H.Z., J.T.), Department of Neurosurgery (J.H.Z.) and Department of Anesthesiology (J.H.Z.), Loma Linda University School of Medicine, Loma Linda, CA.

### Sources of Funding

This work was supported by grants from the National Institutes of Health (R01NS091042) of John H Zhang, and the Key Program of Science and Technology Development of Zhejiang Province (2017C03021) and National Natural Science Foundation of China (81870916) of Jianmin Zhang. (J.H.Z.).

### Disclosures

None.

### Supplementary Material

Data S1  
Tables S1–S2  
Figures S1–S5

## REFERENCES

- Casolla B, Cordonnier C. Is hyperselection of patients the right strategy? *JAMA Neurol.* 2019;76:1426–1427. doi: 10.1001/jamaneurol.2019.0213
- Davis SM, Broderick J, Hennerici M, Brun NC, Diringer MN, Mayer SA, Begtrup K, Steiner T, et al. Hematoma growth is a determinant of mortality and poor outcome after intracerebral hemorrhage. *Neurology.* 2006;66:1175–1181. doi: 10.1212/01.wnl.0000208408.98482.99
- Delcourt C, Huang Y, Arima H, Chalmers J, Davis SM, Heeley EL, Wang J, Parsons MW, Liu G, Anderson CS, et al. Hematoma growth and outcomes in intracerebral hemorrhage: the INTERACT1 study. *Neurology.* 2012;79:314–319. doi: 10.1212/WNL.0b013e318260cbb4
- Withers SE, Parry-Jones AR, Allan SM, Kasher PR. A multi-model pipeline for translational intracerebral haemorrhage research. *Transl Stroke Res.* 2020;11:1229–1242. doi: 10.1007/s12975-020-00830-z
- Appelboom G, Piazza MA, Hwang BY, Carpenter A, Bruce SS, Mayer S, Connolly ES, et al. Severity of intraventricular extension correlates with level of admission glucose after intracerebral hemorrhage. *Stroke.* 2011;42:1883–1888. doi: 10.1161/STROKEAHA.110.608166
- Qureshi AI, Palesch YY, Martin R, Novitzke J, Cruz-Flores S, Ehtisham A, Ezzeddine MA, Goldstein JN, Kirmani JF, Hussein HM, et al. Association of serum glucose concentrations during acute hospitalization with hematoma expansion, perihematomal edema, and three month outcome among patients with intracerebral hemorrhage. *Neurocrit Care.* 2011;15:428–435. doi: 10.1007/s12028-011-9541-8
- Stead LG, Jain A, Bellolio MF, Odufuye A, Gilmore RM, Rabinstein A, Chandra R, Dhillon R, Manivannan V, Serrano LA, et al. Emergency department hyperglycemia as a predictor of early mortality and worse functional outcome after intracerebral hemorrhage. *Neurocrit Care.* 2010;13:67–74. doi: 10.1007/s12028-010-9355-0
- Johnston KC, Bruno A, Pauls QI, Hall CE, Barrett KM, Barsan W, Fansler A, Van de Bruinhorst K, Janis S, Durkalski-Mauldin VL, et al. Intensive vs standard treatment of hyperglycemia and functional outcome in patients with acute ischemic stroke: the shine randomized clinical trial. *JAMA.* 2019;322:326–335. doi: 10.1001/jama.2019.9346
- Roman AC, Carvajal-Gonzalez JM, Merino JM, Mulero-Navarro S, Fernandez-Salguero PM. The aryl hydrocarbon receptor in the cross-road of signalling networks with therapeutic value. *Pharmacol Ther.* 2018;185:50–63. doi: 10.1016/j.pharmthera.2017.12.003
- Juricek L, Coumoul X. The aryl hydrocarbon receptor and the nervous system. *Int J Mol Sci.* 2018;19. doi: 10.3390/ijms19092504
- Rothhammer V, Quintana FJ. The aryl hydrocarbon receptor: an environmental sensor integrating immune responses in health and disease. *Nat Rev Immunol.* 2019;19:184–197. doi: 10.1038/s41577-019-0125-8
- Fernandez-Salguero PM, Ward JM, Sundberg JP, Gonzalez FJ. Lesions of aryl-hydrocarbon receptor-deficient mice. *Vet Pathol.* 1997;34:605–614. doi: 10.1177/030098589703400609
- Cuartero MI, Ballesteros I, de la Parra J, Harkin AL, Abautret-Daly A, Sherwin E, Fernández-Salguero P, Corbí ÁL, Lizasoain I, Moro MA, et al. L-kynurenine/aryl hydrocarbon receptor pathway mediates brain damage after experimental stroke. *Circulation.* 2014;130:2040–2051. doi: 10.1161/CIRCULATIONAHA.114.011394
- Dabir P, Marinic TE, Krukovets I, Stenina OI. Aryl hydrocarbon receptor is activated by glucose and regulates the thrombospondin-1 gene promoter in endothelial cells. *Circ Res.* 2008;102:1558–1565. doi: 10.1161/CIRCRESAHA.108.176990
- Zhang Y, Zhu W, Yu H, Yu J, Zhang M, Pan X, Gao X, Wang Q, Sun H. P2Y4/TSP-1/TGF-beta1/pSmad2/3 pathway contributes to acute generalized seizures induced by kainic acid. *Brain Res Bull.* 2019;149:106–119.
- Argaw AT, Gurfein BT, Zhang Y, Zameer A, John GR. VEGF-mediated disruption of endothelial CLN-5 promotes blood-brain barrier breakdown. *Proc Natl Acad Sci USA.* 2009;106:1977–1982. doi: 10.1073/pnas.0808698106
- Barus R, Bergeron S, Auger F, Laloux C, Skrobala E, Bongiovanni A, Potey C, Bordet R, Chen Y, Gautier S, et al. Sex differences in cognitive impairment induced by cerebral microhemorrhage. *Transl Stroke Res.* 2021;12:316–330. doi: 10.1007/s12975-020-00820-1
- Garcia JH, Wagner S, Liu KF, Hu XJ. Neurological deficit and extent of neuronal necrosis attributable to middle cerebral artery occlusion in rats. Statistical validation. *Stroke.* 1995;26:627–634;discussion 635. doi: 10.1161/01.STR.26.4.627
- Xu P, Hong YE, Xie YI, Yuan K, Li J, Sun R, Zhang X, Shi X, Li R, Wu J, et al. TREM-1 exacerbates neuroinflammatory injury via NLRP3 inflammasome-mediated pyroptosis in experimental subarachnoid hemorrhage. *Transl Stroke Res.* 2021;12:643–659. doi: 10.1007/s12975-020-00840-x
- Zhang C, Jiang M, Wang WQ, Zhao SJ, Yin YX, Mi QJ, Yang MF, Song YQ, Sun BL, Zhang ZY, et al. Selective mGluR1 negative allosteric modulator reduces blood-brain barrier permeability and cerebral edema after experimental subarachnoid hemorrhage. *Transl Stroke Res.* 2020;11:799–811. doi: 10.1007/s12975-019-00758-z
- Matei N, Camara J, McBride D, Camara R, Xu N, Tang J, Zhang JH, et al. Intranasal wnt3a attenuates neuronal apoptosis through Frz1/PIWIL1a/FOXO1 pathway in MCAO rats. *J Neurosci.* 2018;38:6787–6801. doi: 10.1523/JNEUROSCI.2352-17.2018
- Tang XN, Berman AE, Swanson RA, Yenari MA. Digitally quantifying cerebral hemorrhage using Photoshop and Image J. *J Neurosci Methods.* 2010;190:240–243. doi: 10.1016/j.jneumeth.2010.05.004
- Ahmad AS, Mendes M, Hernandez D, Dore S. Efficacy of laropiprant in minimizing brain injury following experimental intracerebral hemorrhage. *Sci Rep.* 2017;7:9489. doi: 10.1038/s41598-017-09994-5
- Nishikawa H, Liu L, Nakano F, Kawakita F, Kanamaru H, Nakatsuka Y, Okada T, Suzuki H, et al. Modified citrus pectin prevents blood-brain barrier disruption in mouse subarachnoid hemorrhage by inhibiting galectin-3. *Stroke.* 2018;49:2743–2751. doi: 10.1161/STROKEAHA.118.021757
- Környey S. Rapidly fatal pontile hemorrhage: clinical and anatomic report. *Arch Neurol Psychiatry.* 1939;41:793–799. doi: 10.1001/archneurpsyc.1939.02270160149012
- Santucci JA, Ross SR, Greenert JC, Aghaei F, Ford L, Hollabaugh KM, Cornwell BO, Wu DH, Zheng B, Bohnstedt BN, et al. Radiological estimation of intracranial blood volume and occurrence of hydrocephalus determines stress-induced hyperglycemia after aneurysmal subarachnoid hemorrhage. *Transl Stroke Res.* 2019;10:327–337. doi: 10.1007/s12975-018-0646-7
- Lamas B, Richard ML, Leducq V, Pham H-P, Michel M-L, Da Costa G, Bridonneau C, Jegou S, Hoffmann TW, Natividad JM, et al. CARD9 impacts colitis by altering gut microbiota metabolism of tryptophan into aryl hydrocarbon receptor ligands. *Nat Med.* 2016;22:598–605. doi: 10.1038/nm.4102
- Saxena A, Anderson CS, Wang X, Sato S, Arima H, Chan E, Muñoz-Venturelli P, Delcourt C, Robinson T, Stapf C, et al. Prognostic significance of hyperglycemia in acute intracerebral hemorrhage: the INTERACT2 study. *Stroke.* 2016;47:682–688. doi: 10.1161/STROKEAHA.115.011627
- Zhang F, Li H, Qian J, Tao C, Zheng J, You C, Yang MU. Hyperglycemia predicts bleed sign in patients with intracerebral hemorrhage. *Med Sci Monit.* 2018;24:6237–6244. doi: 10.12659/MSM.910024
- Liu J, Gao BB, Clermont AC, Blair P, Chilcote TJ, Sinha S, Flaumenhaft R, Feener EP, et al. Hyperglycemia-induced cerebral hematoma expansion is mediated by plasma kallikrein. *Nat Med.* 2011;17:206–210. doi: 10.1038/nm.2295
- Chiu CD, Chen CC, Shen CC, Chin LT, Ma HI, Chuang HY, Cho DY, Chu CH, Chang C, et al. Hyperglycemia exacerbates intracerebral hemorrhage via the downregulation of aquaporin-4: temporal assessment with magnetic resonance imaging. *Stroke.* 2013;44:1682–1689. doi: 10.1161/STROKEAHA.113.675983
- Esser C, Lawrence BP, Sherr DH, Perdew GH, Puga A, Barouki R, Coumoul X. Old receptor, new tricks—the ever-expanding universe of aryl hydrocarbon receptor functions. Report from the 4th AHR meeting, 29(-)31 August 2018 in Paris, France. *Int J Mol Sci.* 2018;19:3603.
- Xu K, Yang Z, Shi R, Luo C, Zhang Z. Expression of aryl hydrocarbon receptor in rat brain lesions following traumatic brain injury. *Diagn Pathol.* 2016;11:72. doi: 10.1186/s13000-016-0522-2
- Jacob A, Potin S, Chapy H, Crete D, Glacial F, Ganeshamoorthy K, Couraud PO, Scherrmann JM, Declèves X, et al. Aryl hydrocarbon receptor regulates CYP1B1 but not ABCB1 and ABCG2 in hCMEC/D3 human cerebral microvascular endothelial cells after TCDD exposure. *Brain Res.* 2015;1613:27–36. doi: 10.1016/j.brainres.2015.03.049
- Matsumoto K, Kinoshita K, Yoshimizu A, Kurauchi Y, Hisatsune A, Seki T, Katsuki H, et al. Laquinimod and 3,3'-diindolylethane alleviate neuropathological events and neurological deficits in a mouse model of intracerebral hemorrhage. *J Neuroimmunol.* 2020;342:577195. doi: 10.1016/j.jneuroim.2020.577195

- 
36. Freeze WM, Jacobs HIL, Schreuder FHBM, van Oostenbrugge RJ, Backes WH, Verhey FR, Klijn CJM, et al. Blood-brain barrier dysfunction in small vessel disease related intracerebral hemorrhage. *Front Neurol*. 2018;9:926. doi: 10.3389/fneur.2018.00926
  37. Silva Y, Leira R, Tejada J, Lainez JM, Castillo J, Davalos A, et al. Molecular signatures of vascular injury are associated with early growth of intracerebral hemorrhage. *Stroke*. 2005;36:86–91. doi: 10.1161/01.STR.0000149615.51204.0b
  38. Chen W-C, Chang L-H, Huang S-S, Huang Y-J, Chih C-L, Kuo H-C, Lee Y-H, Lee I-H, et al. Aryl hydrocarbon receptor modulates stroke-induced astrogliosis and neurogenesis in the adult mouse brain. *J Neuroinflammation*. 2019;16:187. doi: 10.1186/s12974-019-1572-7
  39. Jiang N, Zhang Z, Shao X, Jing R, Wang C, Fang W, et al. Blockade of thrombospondin-1 ameliorates high glucose-induced peritoneal fibrosis through downregulation of Tgf-beta1/Smad3 signaling pathway. *J Cell Physiol*. 2020;235:364–379.
  40. Di Biase S, Shim HS, Kim KH, Vinciguerra M, Rappa F, Wei M, Brandhorst S, Cappello F, Mirzaei H, Lee C, et al. Fasting regulates EGR1 and protects from glucose- and dexamethasone-dependent sensitization to chemotherapy. *PLoS Biol*. 2017;15:e2001951. doi: 10.1371/journal.pbio.2001951

# **SUPPLEMENTAL MATERIAL**

## Data S1.

### Supplemental Materials & Methods

#### **Intracerebroventricular injection**

Using clustered regularly interspaced short palindromic repeat/Cas9 (CRISPR/Cas9) technology, we edited the *in vivo* genome mediated by homology-independent targeted integration. We used AHR CRISPR/Cas9 KO Plasmid (sc-419054, Santa Cruz) to inhibit AHR expression in the mouse brain and TSP-1 CRISPR Activation Plasmid (sc-423381-ACT, Santa Cruz) to activate TSP-1 expression in the mouse brain. The CRISPR 20 $\mu$ g was suspended in 20 $\mu$ L of transfection medium (sc-108062, Santa Cruz) and then activated using 20 $\mu$ L transfection reagent (sc-395739, Santa Cruz) to get a final concentration 0.5  $\mu$ g/ $\mu$ L of CRISPR. For each of the CRISPRs, a total of 2 $\mu$ L CRISPR was injected into the left lateral ventricle 48h before ICH.

#### **Tail Bleeding Monitoring**

Hemostasis was assessed by measuring bleeding time using the tail transection test. Tail transection (at 2 mm tail diameter) was performed 30 minutes after the end of collagenase, vehicle (DMSO), or TMF administration, and the bleeding times (visual observation) were recorded.

#### ***Ex Vivo* Thrombus Formation**

A modified *ex vivo* clot formation model was used. In brief, three groups of mice were used here, namely ICH+Dx+DMSO, ICH+Dx+TMF, and *ex vivo* TMF groups. For mice in DMSO and *ex vivo* TMF groups, whole blood was harvested by cardiac puncture, and 200  $\mu$ L of the blood was mixed and vortexed with 600  $\mu$ L of DMSO *ex vivo* or 600  $\mu$ L of 100  $\mu$ M TMF *ex vivo*. For mice in the ICH+Dx+TMF group, 800  $\mu$ L of whole blood was harvested via cardiac puncture. Samples were kept at room temperature for 2 minutes, followed by centrifugation for 30 seconds at 4,000 g. The tubes were gently removed and the amount of uncoagulated supernatant was quantified.

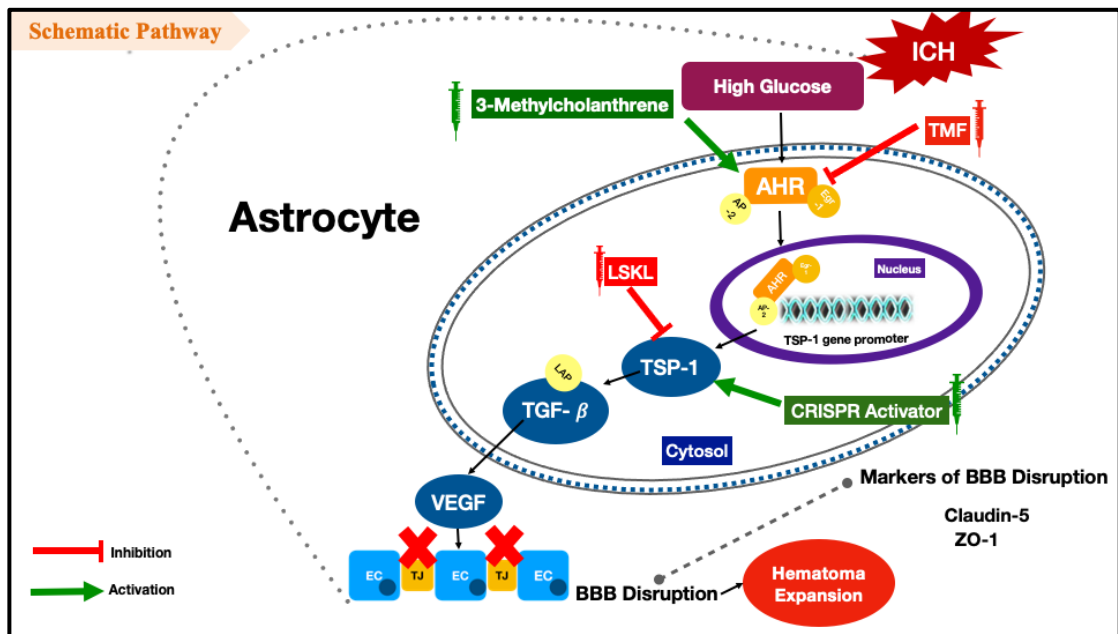
**Table S1. Animal use and mortality rate**

<b>Group</b>	<b>Mortality</b>	<b>Subtotal</b>
<b>Experiment 1</b>		
Sham	0% (0/6)	6
ICH (6, 24, 72h)	0% (0/18)	18
ICH+Dx (6, 24, 72h)	0% (0/18)	18
ICH+Mannitol 24h	0% (0/6)	6
<b>Experiment 2</b>		
Sham	0% (0/8)	8
ICH (6, 12, 24, 72h)	0% (0/26)	26
ICH+Dx (6, 12, 24, 72h)	0% (0/26)	26
<b>Experiment 3</b>		
Sham	0% (0/24)	24
ICH	0% (0/12)	12
ICH+TMF	0% (0/6)	6
ICH+Dx	3.7% (1/26+1)	27
ICH+Dx+DMSO	5.3% (2/36+2)	38
ICH+Dx+TMF (1.5mg/kg)	7.7% (1/12+1)	13
ICH+Dx+TMF (5mg/kg)	0% (0/50)	50
ICH+Dx+TMF (15mg/kg)	0% (0/12)	12
<b>Experiment 4</b>		
Sham	0% (0/18) #	0
ICH+Dx	5.2% (1/18+1) #	0
ICH+Dx+AHR CRISPR KO	0% (0/18)	18
ICH+Dx+CRISPR Control	14.3% (2/12+2)	14
<b>Experiment 5</b>		
Sham	0% (0/12) @#	0
ICH	0% (0/18) @#	6
ICH+Dx	0% (0/18) @#	0
ICH+3-MC	14.3% (2/12+2)	14
<b>Experiment 6</b>		
Sham	0% (0/6) @	0
ICH+Dx	0% (0/6) @	0
ICH+Dx+DMSO	0% (0/6)	6
ICH+Dx+TMF	14.3% (0/6)	6
ICH+Dx+TMF+CRISPR Control	0% (0/6)	6
ICH+Dx+TMF+TSP-1 CRISPR Activation	14.3% (1/6+1)	7
ICH+Dx+3-MC	14.3% (1/6+1)	7
ICH+Dx+3-MC+DMSO	14.3% (1/6+1)	7
ICH+Dx+3-MC+LSKL	0% (0/6)	6
<b>Total</b>	<b>3.1%</b>	<b>387</b>

**Table S2. Antibodies used in Western blot and Immunohistochemistry**

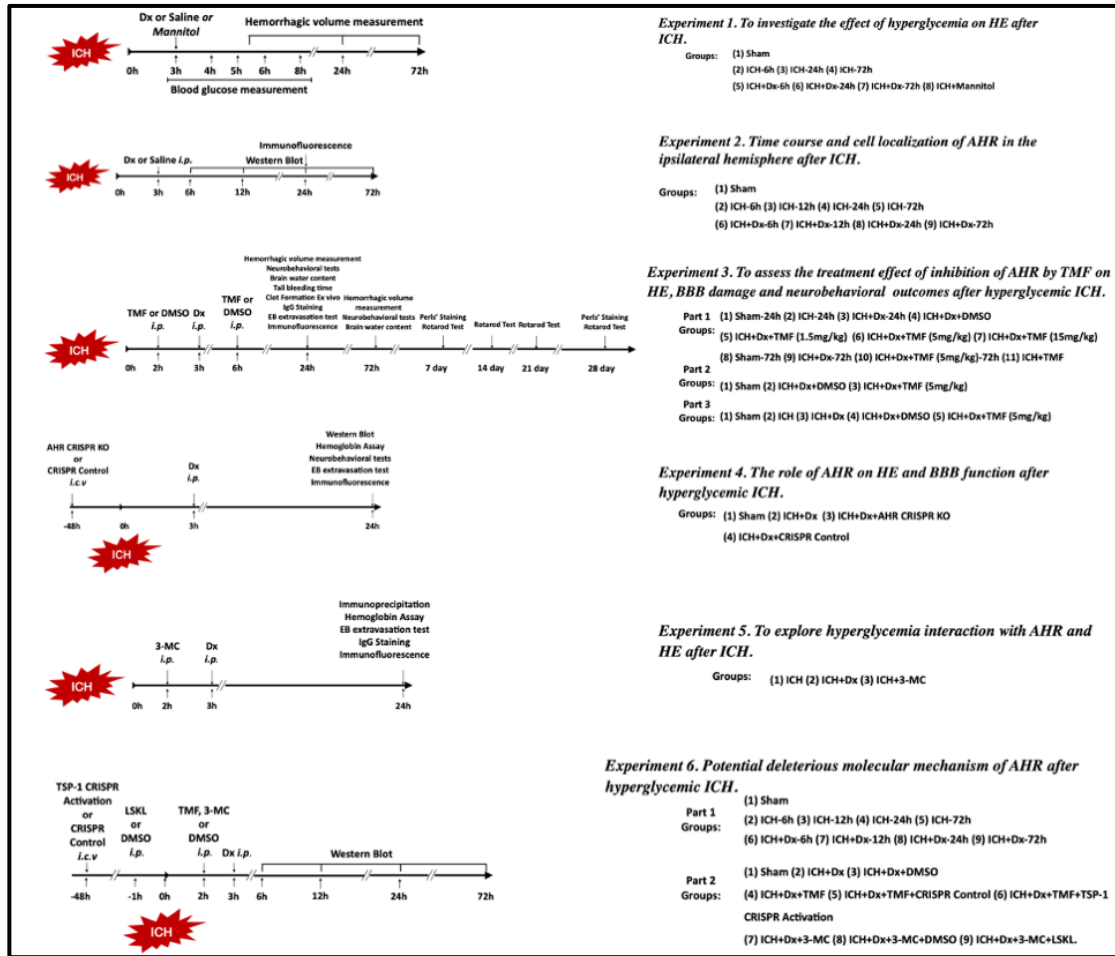
<b>Species and Name</b>	<b>Dilution rate</b>	<b>Manufacture</b>
Rabbit polyclonal Anti-AHR antibody	1:500	ab84833, Abcam
Rabbit polyclonal Anti-TSP-1 antibody	1:1000	ab85762, Abcam
Rabbit polyclonal Anti-TGF- $\beta$ antibody	1:1000	ab92486, Abcam
Rabbit polyclonal Anti-VEGFA antibody	1:1000	ab46154, Abcam
Rat monoclonal Anti-ZO-1 antibody	1:1000	sc-33725, Santa Cruz
Rabbit monoclonal Anti-Claudin 5 antibody	1:1000	ab131259, Abcam
Mouse polyclonal Anti- $\beta$ -actin	1:3000	sc-47778, Santa Cruz
Mouse monoclonal Egr-1 antibody	-	sc-515830, Santa Cruz
Protein A/G PLUS- Agarose	-	sc-2003, Santa Cruz
Anti-glial fibrillary acidic protein	1:100	Santa Cruz
Anti-VWF antibody	1:100	Santa Cruz

**Figure S1. Graphic schematic pathway.**



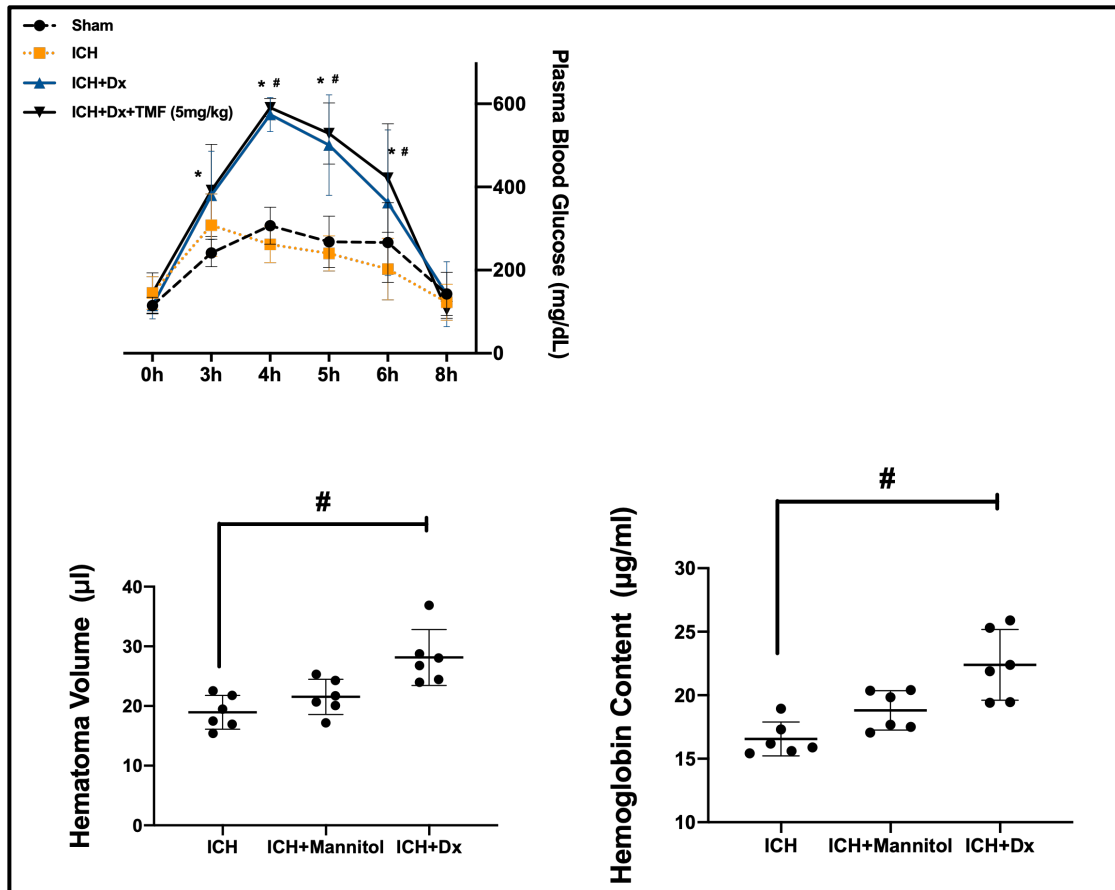
The effects of AHR inhibition on hematoma expansion and underlying mechanisms of protection pertaining to BBB protection after hyperglycemic ICH in mice. The cell type in representative figure is astrocyte. AHR, aryl hydrocarbon receptor; ICH, intracerebral hemorrhage; BBB, blood-brain barrier; TMF, trimethoxyflavone; CRISPR, clustered regularly interspaced short palindromic repeat; KO, knockout; TSP-1, thrombospondin-1; TGF- $\beta$ , transforming growth factor- $\beta$ ; VEGF, vascular endothelial growth factor; ZO-1, zonula occludens-1; EC, endothelial cells; TJ, tight junction.

**Figure S2. Experiment and study groups design.**



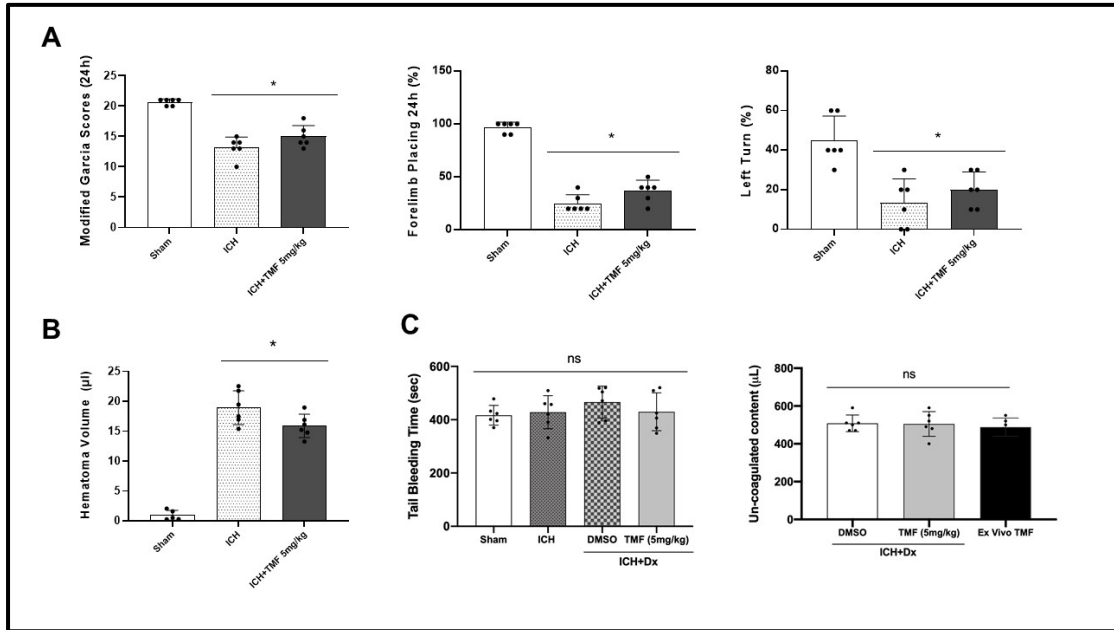
ICH, intracerebral hemorrhage; Dx, dextrose; HE, hematoma expansion; AHR, aryl hydrocarbon receptor; BBB, blood-brain barrier; DMSO, dimethyl sulfoxide; TMF, trimethoxyflavone; CRISPR, clustered regularly interspaced short palindromic repeat; KO, knockout;

**Figure S3. Temporal plasma glucose changes and hemorrhagic volume comparison in different groups.**



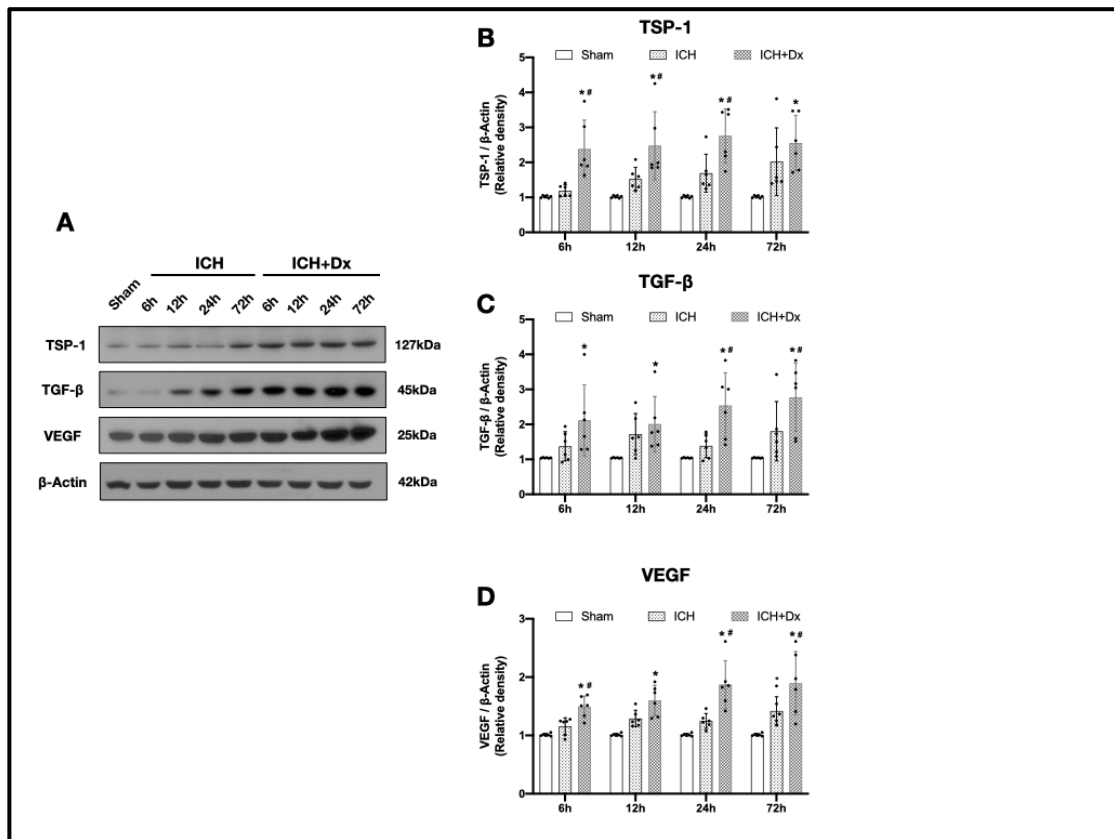
(A) Plasma glucose measured using glucometer by tail-tip transection in different groups. Sham group was shared between 6h, 24h and 72h. The error bars represent mean  $\pm$  SD. \*  $P < 0.05$  vs Sham. #  $P < 0.05$  vs ICH.  $n = 6$  for each group. Two-way ANOVA, Tukey's test. (B-C) Statistical analysis of hematoma volume and hemoglobin assay in ICH, ICH+Mannitol and ICH+Dx group at 24h after ICH. The error bars represent mean  $\pm$  SD. #  $P < 0.05$  vs ICH.  $n = 6$  for each group. Kruskal-Wallis test, Dunn's test. ICH, intracerebral hemorrhage; Dx, dextrose; TMF, trimethoxyflavone.

**Figure S4. TMF had no effect on neurobehavioral function, hematoma volume and hemostasis in ICH mice at 24h.**



(A-B) Statistical analysis of modified garcia test, forelimb placing, corner turn test and hematoma volume in Sham, ICH, ICH+TMF group at 24h after ICH. (C) Tail bleeding time in different groups 30 min after administration. Un-coagulated content measurement ex vivo in different groups. The error bars represent mean  $\pm$  SD. \*  $P < 0.05$  vs Sham. ns, no statistical difference.  $n = 6$  for each group. Kruskal-Wallis test, Dunn's test. ICH, intracerebral hemorrhage; DMSO, dimethyl sulfoxide; TMF, trimethoxyflavone.

**Figure S5. Temporal expressions of TSP-1, TGF- $\beta$  and VEGF in ICH group and ICH+Dx group.**



(A) Representative and quantitative analysis (B-D) of western blot bands showing temporal expressions of TSP-1, TGF- $\beta$  and VEGF at 6h, 12h, 24h, 72h in ICH group and ICH+Dx group. Sham group was shared between 6h, 24h, 72h. The error bars represent mean $\pm$ SD. \*  $P < 0.05$  vs Sham. #  $P < 0.05$  vs ICH. Two-way ANOVA, Tukey's test. ICH, intracerebral hemorrhage; Dx, dextrose; TSP-1, thrombospondin-1; TGF- $\beta$ , transforming growth factor- $\beta$ ; VEGF, vascular endothelial growth factor.